Polar discontinuities and interfacial electronic properties of Bi_2O_2Se on $SrTiO_3$

Ziye Zhu,[1,2,3] Jingshan Qi,[4] Xiaorui Zheng,[2,3] Xiao Lin,[5] and Wenbin Li[2,3,*]

[1]*School of Materials Science and Engineering, Zhejiang University, Hangzhou 310027, China*

[2]*Key Laboratory of 3D Micro/Nano Fabrication and Characterization of Zhejiang Province, School of Engineering, Westlake University, Hangzhou 310030, China*

[3]*Research Center for Industries of the Future, Westlake University, Hangzhou 310030, China*

[4]*School of Science, Tianjin University of Technology, Tianjin 300384, China*

[5]*Key Laboratory for Quantum Materials of Zhejiang Province, School of Science, Westlake University, Hangzhou 310030, China*

(Received 10 August 2023; revised 22 November 2023; accepted 6 December 2023; published 20 December 2023)

The layered oxychalcogenide semiconductor Bi_2O_2Se (BOS) hosts a multitude of unusual properties including high electron mobility. Owing to similar crystal symmetry and lattice constants, the perovskite oxide $SrTiO_3$ (STO) has been demonstrated to be an excellent substrate for wafer-scale growth of atomically thin BOS films. However, the structural and electronic properties of the BOS/STO interface remain poorly understood. Here, through first-principles study, we reveal that polar discontinuities and interfacial contact configurations have a strong impact on the electronic properties of ideal BOS/STO interfaces. The lowest-energy [Bi-TiO_2] contact type, which features the contact between a Bi_2O_2 layer of BOS with the TiO_2-terminated surface of STO, incurs significant interfacial charge transfer from BOS to STO, producing a BOS/STO-mixed, *n*-type metallic state at the interface. By contrast, the [Se-SrO] contact type, which is the most stable contact configuration between BOS and SrO-terminated STO substrate, has a much smaller interfacial charge transfer from STO to BOS and exhibits *p*-type electronic structure with no interfacial hybridization between BOS and STO. These results indicate that BOS grown on TiO_2-terminated STO substrates could be a fruitful system for exploring emergent phenomena at the interface between an oxychalcogenide and an oxide, whereas BOS grown on SrO-terminated substrates may be more advantageous for preserving the excellent intrinsic transport properties of BOS.

DOI: 10.1103/PhysRevB.108.245304

I. INTRODUCTION

Bismuth oxyselenide Bi_2O_2Se (BOS) has recently emerged as a layered semiconductor with a moderate bandgap ($E_g \sim 0.8$ eV), excellent air stability, ultrahigh electron mobility, and extraordinary optical sensitivity [1–4]. Room-temperature electron Hall mobility as high as 450 $cm^2V^{-1}s^{-1}$ has been measured in BOS ultrathin films (thickness ~6 nm) grown by chemical vapor deposition (CVD) [1]. At low temperatures, the electron mobility of such BOS thin films can reach a huge number above 20 000 $cm^2V^{-1}s^{-1}$ [1], rivaling that of two-dimensional (2D) electron gas at the $LaAlO_3/SrTiO_3$ (LAO/STO) interface, as well as graphene samples grown by CVD [5,6]. A huge static dielectric constant ($\epsilon_0 > 150$), which results from the proximity to a ferroelectric transition and strongly suppresses Coulombic defect scattering, is crucial for the observed ultrahigh electron mobility [7,8]. Moreover, high-quality, stable native oxide dielectric Bi_2SeO_5 can directly form on top of BOS via layer-by-layer oxidization while preserving the high electron mobility of BOS, presenting a unique advantage of BOS over other 2D materials in terms of compatibility with existing silicon-based semiconductor technology [9].

For commercial success, functional BOS devices need to be produced at large scale and with uniform characteristics. Important in this respect, it has recently been shown that high-quality, single-crystalline BOS thin films and atomic layers can be grown on STO substrates at wafer scale using CVD or molecular beam epitaxy [10,11], owing to the symmetry and lattice matching between BOS and STO. However, the measured electron Hall mobility of BOS thin films grown on STO substrates (~94 $cm^2V^{-1}s^{-1}$) was found to be poorer than those grown on mica substrates (200–450 $cm^2V^{-1}s^{-1}$) [10]. Although interfacial scattering was proposed as a possible explanation of the mobility degradation, the exact microscopic origin remains unclear. Furthermore, unlike conventional layered semiconductors such as MoS_2, whose layers are bound together by van der Waals (vdW) interaction, BOS features electrostatic interaction between positively charged Bi_2O_2 layers and negatively charged Se layers. This feature could lead to stronger interfacial bonding and interaction between BOS and STO than those between a conventional vdW layered semiconductor and STO, resulting in richer interfacial phenomena. Indeed, the close symmetry and lattice-constant matching between BOS and STO, as well as between BOS and other perovskite-related materials [7], could enable the growth of a wide range of BOS-based artificial heterostructures with emergent properties. In the past, exotic phenomena such as interface superconductivity, strong electromagnetic coupling, and fractional quantum Hall effect have been observed at the interfaces of two perovskite oxides such as between LAO and STO [12]. By contrast, little has been explored with respect to the interfacial properties between an

*liwenbin@westlake.edu.cn

oxychalcogenide (to which BOS belongs) and a perovskite oxide.

These attractive prospects have motivated us to investigate the structural and electronic properties of ideal BOS/STO interfaces via first-principles calculations. The results of our study reveal that interfacial contact configurations have a strong influence on the electronic properties of the BOS/STO interfaces, which originates from the discontinuity of polarity ("polar discontinuity") at the interface between BOS and STO. As a result of the polar discontinuity and the subsequent electronic reconstruction, the lowest-energy [Bi-TiO_2] interface, formed between a Bi_2O_2 layer of BOS and a TiO_2-terminated surface of STO, features a significant amount of interfacial charge transfer from BOS to STO, producing an *n*-type, BOS/STO-mixed metallic state at the interface. In contrast, the [Se-SrO] contact type, which is the most stable contact configuration between BOS and SrO-terminated STO substrate, belongs to *p*-type and has a much smaller interfacial charge transfer from STO to BOS, with no noticeable interfacial electronic hybridization. These results have important implications for exploring emergent phenomena at the interfaces of oxychalcogenides and oxides, as well as for optimizing the epitaxial growth of BOS thin films on oxide substrates for practical device applications.

II. METHODS

For our calculations, we adopted density functional theory (DFT) as implemented in the Vienna *ab initio* simulation package (VASP) [14]. The interaction between valence electrons and ionic cores was treated using projector augmented wave potentials [13]. The exchange-correlation functional within the generalized gradient approximation (GGA) as parametrized by Perdew, Burke, and Ernzerhof (PBE) [15] was used. We have tested the GGA+U method [16,17] with $U = 4.36$ eV for the Ti $3d$ states in STO [18]. The GGA+U calculations lead to qualitatively the same results as those obtained using the PBE functional.

To study the properties of ideal BOS/STO interface, we constructed a heterostructural model consisting of BOS and STO slabs along each of their [001] directions. The tetragonal supercell of the slab model corresponds to an in-plane repeating unit of 1×1 for both BOS and STO, and the in-plane lattice constant of the supercell follows the experimental lattice constant of STO [19], which simulates the coherent epitaxial growth of ultrathin BOS films on thick STO substrates [10,11]. Regarding the specific atomistic arrangement at the interface, we considered all possible interfacial contact configurations and a series of corresponding slab models were constructed and simulated, in order to determine the lowest-energy configurations. The STO layers in the slab model is always stoichiometric. Hence, depending on the interfacial contact configurations, the surface terminations of STO slabs vary on the vacuum side. The surface of the BOS slab on the vacuum side is terminated by a layer of Se atoms passivated by hydrogens. The reason we use this configuration is that real BOS (001) surface usually consists of a half-full, dimerized Se layer with 50% of vacancies [2]. We find that hydrogen passivation of a full Se surface layer can effectively model the electronic properties of a BOS slab with 50% of surface Se vacancies (see Fig. S1 in the Supplemental Material [20]), while circumventing the need to enlarge the in-plane unit cells of the slab, which significantly reduces the cost of computing the properties of BOS/STO interface. The chemical formulas corresponding to the slab models are $(Bi_2O_2Se)_4H/(SrTiO_3)_3$ and $(Bi_2O_2Se)_3SeH/(SrTiO_3)_3$ for interfaces with a Bi_2O_2 contact layer and Se contact layer, respectively. The slab thickness was verified to be sufficient for modeling the electronic properties of the BOS/STO interfaces (see Fig. S2 in the Supplemental Material [20]).

A sufficiently large vacuum thickness of 20 Å was set in the slab model. Additional dipole correction [21] on the electrostatic potential along the vertical direction of the slab was found to have a negligible influence on the calculated properties. For the plane-wave expansion of the electronic wave functions, a kinetic energy cutoff of 500 eV is used. The Brillouin zone was sampled using a $9\times9\times1$ Monkhorst-Pack **k**-point mesh [22]. The convergence threshold for the self-consistency of the total energy is set to 10^{-4} eV, and all atoms in the slab were fully relaxed until the force on each atom is smaller than 0.01 eV $Å^{-1}$.

III. RESULTS

A. Structure and energetics of the BOS/STO interfaces

As our goal is to understand the interfacial properties of BOS/STO, we begin with a discussion of the crystal structures of both BOS and STO. BOS has a body-centered tetragonal structure with a fourfold symmetry ($I4/mmm$ space group), with the experimental lattice parameters $a = 3.88$ Å, and $c = 12.16$ Å [23]. The corresponding DFT-relaxed lattice constants are $a = 3.93$ Å and $c = 12.33$ Å, which slightly overestimate the experimental values. The structure belongs to the *anti*-$ThCr_2Si_2$ type [24], and the corresponding atomistic model is illustrated in Fig. 1(a) (left panel). In BOS, Bi and O atoms form layered, covalently bonded frameworks with edge-sharing BiO_4 square-pyramid coordination [7,24]. Between the Bi_2O_2 layers are Se atoms arranged in a 2D square lattice. As Se is more electronegative than Bi, the Bi atoms in the Bi_2O_2 layers transfer electrons to the Se layers, resulting in positively charged $[Bi_2O_2]_n^{2n+}$ layers and negatively charged $[Se]_n^{2n-}$ layers, where n is the number of repetitive in-plane formula units. The $[Bi_2O_2]_n^{2n+}$ and $[Se]_n^{2n-}$ layers are bound together by forces mostly of electrostatic nature. Since the nominal charge state of Bi in BOS is +3, each Bi atom has a lone pair of $6s^2$ electrons. The lone pair electrons are stereoactive and direct in the layer-normal direction, playing a key role in stabilizing the layered structure [25].

The natural cleavage plane of BOS is the (001) plane. The cleavage process leaves 50 percent of Se on each of the two resulting surfaces, where most of the Se atoms left on the surfaces have a dimerized structure [2]. The interlayer binding energy corresponding to this dimerized "zipper" cleavage mode [26] has a small value of ∼39 meV/$Å^2$, as obtained from our DFT calculations. By contrast, the DFT-calculated binding energy between atomically flat Bi_2O_2 and Se layers, which corresponds to all the Se atoms on one side of the two surfaces created by cleavage, has a much higher value of ∼123 meV/$Å^2$. To put these numbers in perspective, the interlayer binding energy of MoS_2 is merely ∼20 meV/$Å^2$

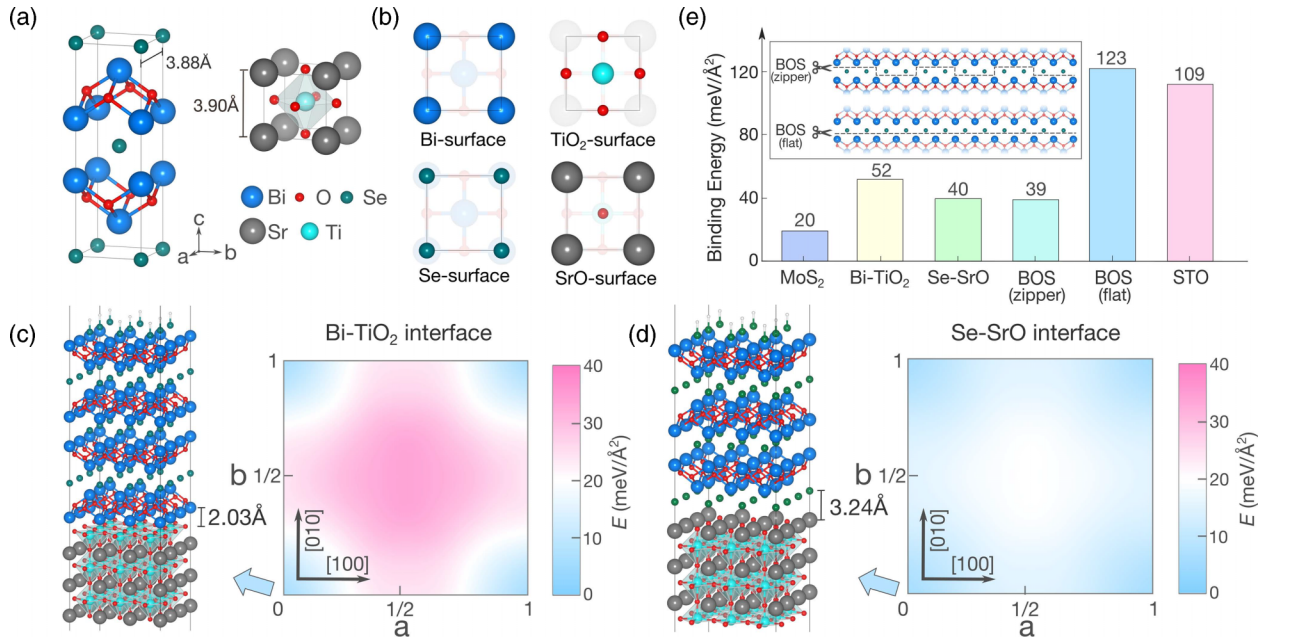

FIG. 1. (a) Atomistic models of the conventional tetragonal unit cell of Bi_2O_2Se (BOS) and the cubic unit cell of $SrTiO_3$ (STO). (b) Illustrations of the Bi- and Se-terminated surfaces of BOS (top- and bottom-left panels), as well as the TiO_2- and SrO-terminated surfaces of STO (top- and bottom-right panels). The representations of atoms are the same as those in (a). (c), (d) DFT-relaxed atomistic structural models of the lowest-energy [Bi-TiO_2] interface (c) and [Se-SrO] interface (d). The distance between the Bi layer and TiO_2 layer at the [Bi-TiO_2] interface is ∼2.0 Å, whereas the distance between the Se layer and SrO layer at the [Se-SrO] interface is ∼3.2 Å. Also shown together are the corresponding changes of the interfacial binding energies with respective to the rigid relative in-plane displacements of BOS and STO slabs along the *a* and *b* axes ([100] and [010] directions). (e) Interlayer/interface binding energies of various systems calculated by density functional theory (DFT). The plot includes data for interlayer binding energy in MoS_2, interface binding energies between BOS and STO that belong to the [Bi-TiO_2] and [Se-SrO] contact types, interlayer binding energies in BOS that correspond to zipper or flat cleavage, as well as the interlayer binding energy between the TiO_2 and SrO sheets in STO. The inset illustrates the contact breaking patterns of the zipper and flat cleavage of BOS.

[27]. The distinct bonding characteristics of BOS suggest that its interfacial properties could be rather different from those of conventional layered semiconductors.

On the other hand, STO has a typical cubic perovskite structure with $Pm\bar{3}m$ space group and an experimental lattice constant of 3.90 Å [19] (the DFT relaxed value is 3.94 Å). The structure of STO is also illustrated in the right panel of Fig. 1(a). In the [001] direction, STO has alternate stacking of planar TiO_2 and SrO atomic sheets. Thus, the (001) surface of STO has two distinct terminations, either TiO_2- or SrO-terminated. As the nominal charge of Sr, Ti, and O in STO are +2, +4, and −2, respectively, in the simple ionic limit, each TiO_2 or SrO sheet can be considered charge neutral [12]. Normally, the surface of STO substrates obtained by cleavage or cutting consists of an equal amount of TiO_2- and SrO-terminated domains separated by half-unit-cell steps [28]. However, simple chemical treatment methods have been developed to achieve fully TiO_2-terminated surfaces [29–31]. The opposite single-terminated SrO surfaces can be obtained either by annealing STO substrates in air at high temperatures [32], or by depositing a SrO monolayer on top of a single-terminated TiO_2 surface [12,33].

The (001) planes of BOS and STO are symmetry matched (both have 2D square lattices), with a small lattice-constant difference of 0.5% (3.88 Å versus 3.90 Å). Therefore, when a BOS thin film is grown on the (001) surface of a STO substrate, coherent interface can form, wherein the in-plane lattice constants of BOS follow those of STO [10,11]. Since the (001) surface of STO can be TiO_2- or SrO-terminated, whereas that of BOS can be terminated with a Bi_2O_2 or Se layer, as illustrated in Fig. 1(b), four atomically sharp interfacial contact types are theoretically possible between BOS and STO. The [Bi-TiO_2] contact type involves the direct contact of a Bi_2O_2 layer of BOS on top of a TiO_2-terminated STO. This contact type has been experimentally observed in BOS thin films grown on STO by both CVD and molecular beam epitaxy [10,11]. The [Se-SrO] contact type corresponds to a Se layer of BOS on SrO-terminated STO. The [Se-TiO_2] and [Bi-SrO] contact types have similar connotations.

In each of the four contact types, additional in-plane translational degrees of freedom exist. We have considered all the possible high-symmetry, coherent interfacial contact configurations between the (001) surfaces of BOS and STO, and carried out DFT calculations of the corresponding interfacial binding energies. Here, the interfacial binding energy (E_{binding}) is defined as the energy per area needed to separate an interface, expressed as $E_{\text{binding}} = \frac{1}{A}(E_{\text{BOS}} + E_{\text{STO}} - E_{\text{slab}})$, where A is the area of the interface. The results of our calculations indicate that the [Bi-TiO_2] contact type, in its most stable configuration, has the highest binding energy of 52 meV/Å^2 among all four interfacial contact types. The binding energy of the [Se-SrO] interface has a close value of 40 meV/Å^2.

In contrast, the other two interfacial contact types, namely [Se-TiO_2] and [Bi-SrO], have much smaller binding energies of 16 meV/Å^2 and 5 meV/Å^2, respectively. Hence, when BOS is grown on a TiO_2-terminated STO substrate, the equilibrium interfacial contact type should be [Bi-TiO_2], which is inconsistent with previous experimental observations [10,11]. On the other hand, if the STO substrate is SrO-terminated, the [Se-SrO] contact type should be energetically much more competitive than the [Bi-SrO] type. The energetic order between different contact types can be understood in terms of their interfacial charge transfer properties, which will be discussed latter.

The lowest-energy in-plane alignments between BOS and STO in the [Bi-TiO_2] and [Se-SrO] contact types are in accordance with the illustrated Bi and Se surfaces of BOS, as well as the TiO_2 and SrO surfaces of STO in Fig. 1(b). Specifically, in the [Bi-TiO_2] contact type, the Bi atoms of BOS sit above the four-fold hollow sites of O atoms and align with the Sr atoms below, in agreement with experimental observations [10,11]. On the other hand, in the [Se-SrO] contact type, Se atoms are located directly on top of Sr atoms. Additional side views of the [Bi-TiO_2] and [Se-SrO] contact types are shown in Figs. 1(c) and 1(d) and Supplemental Fig. S3.

In Fig. 1(e) we compare the binding energies of [Bi-TiO_2] and [Se-SrO] interfaces with the interfacial or interlayer binding energies in other systems, including the vdW interlayer binding energy of MoS_2, the interlayer binding energy of BOS that corresponds to zipper or atomically flat cleavage, as well as the binding energy between TiO_2 and SrO sheets in STO. It is noted that in the flat cleavage mode of BOS, which leaves all Se atoms on one side of the cleaved surface, the corresponding binding energy (123 meV/Å^2) is even larger than that of between TiO_2 and SrO sheets in STO (109 meV/Å^2). This shows that the interlayer electrostatic interaction between $[Bi_2O_2]_n^{2n+}$ and $[Se]_n^{2n-}$ layers in BOS is by no means weak. Furthermore, the binding energies of the [Bi-TiO_2] and [Se-SrO] interfaces are both several times higher than that between MoS_2 layers. The relatively strong interfacial binding between BOS and STO, in combination with symmetry and close lattice-constant matching, makes coherent epitaxial growth of BOS on STO and other perovskite-related materials growth possible [10,11]. This creates an exciting opportunity to generate a large variety of novel heterostructures between the oxychalcogenide BOS and perovskite oxides.

B. Electronic properties of the ideal BOS/STO interfaces

Having studied the contact configurations and energetics of the BOS/STO interfaces, we next investigate their electronic properties. The DFT-calculated electronic band structures of bulk BOS and STO using the PBE exchange-correlation functional are shown in Supplemental Fig. S4(a,b). The calculated bandgaps of bulk BOS and STO are 0.53 and 1.94 eV, respectively, which underestimate the corresponding experimental values of 0.8 eV [2] and 3.25 eV [35], as is typical for bandgaps obtained from DFT-PBE calculations. We also calculated the band structure of bulk STO by using the GGA+U method ($U = 4.36$ eV for the Ti 3d states [18]). The result is shown in Supplemental Fig. S4(c), from which the GGA+U bandgap of STO is determined to be 2.51 eV.

Figures 2(a) and 2(b) show the DFT-computed electronic band structures of the heterostructural slab models of the [Bi-TiO_2] and [Se-SrO] interfaces, which correspond to the atomistic structural models in Figs. 1(c) and 1(d), respectively. The GGA+U band structures are shown in Supplemental Fig. S5, showing qualitatively the same features. In the case of the [Bi-TiO_2] interface, the Fermi level (E_F) is located above the conduction band minimum (CBM) and crosses both the BOS and STO components, resulting in an n-type metallic phase. Notably, there is a distinct hybridization of electronic states between BOS and STO near the E_F along the M–Γ and X–M directions in its 2D Brillouin zone. On the other hand, for the [Se-SrO] contact interface, the E_F shifts to the valence band, resulting in a p-type metallic state. However, no noticeable hybridization between BOS and STO can be observed from the projected band structure in this contact type.

The difference in interfacial electronic hybridization between the [Bi-TiO_2] and [Se-SrO] contact types is further analyzed through layer-by-layer projected density of states (PDOS) of the electronic states near the Fermi level, as shown in Fig. 3, where the PDOS are resolved into the contributions from the s, p, d orbitals of the atoms in each atomic layer of the heterostructures. In the [Bi-TiO_2] contact type, the PDOS near the Fermi level has a major contribution from the Ti d_{z^2} orbital in the TiO_2 layer at the interface, in addition to the Ti d_{xz} and d_{yz} orbitals [Fig. 3(a)]. The p orbital of the Bi atoms in the Bi_2O_2 layer at the interface, mainly of the p_z character [7], also has a significant contribution to the PDOS. Normally, the CBM of pristine STO derives only from the t_{2g} manifold of the Ti 3d states [36], that is, the d_{xz}, d_{yz}, and d_{xy} orbitals. The appearance of the contribution from d_{z^2} orbital to the PDOS near the Fermi level indicates the hybridization of the d_{z^2} orbital of the interfacial Ti atoms with the p_z orbital of the Bi atoms at the [Bi-TiO_2] interface. This is in contrast to the 2D electron gas at the LAO/STO interface, where the charge is localized in a split-off d_{xy} orbital of the interfacial Ti atoms [37]. As for the [Se-SrO] contact type, Fig. 3(b) shows that the SrO layer at the interface has no contribution to the PDOS at the Fermi level, consistent with the absence of interfacial hybridization for this contact type.

To probe the origin of the metallic states of the BOS/STO interfaces, we compute the electronic band structures of isolated slabs of BOS and STO. Supplemental Fig. S6 shows that the Fermi levels of STO slabs are always located in the band gap regardless of the surface termination, corresponding to an insulating state. In contrast, in a Bi_2O_2-terminated BOS slab, the Fermi levels move into the conduction band, while in a Se-terminated slab, the Fermi level is in the valence band. The alignment of the valence band maximum (VBM) and CBM of the BOS and STO slabs before forming a heterostructure is shown in Supplemental Fig. S7. When a BOS slab and a STO slab are put into contact, charge transfer can occur between BOS and STO slabs in order to reach a uniform electron chemical potential across the interface. In the case of [Bi-TiO_2] interface, after electronic reconstruction, the Fermi level crosses the conduction bands of both BOS and STO, indicating charge transfer from the BOS slab to the STO slab, while in the case of [Se-SrO] interface, the Fermi level crosses

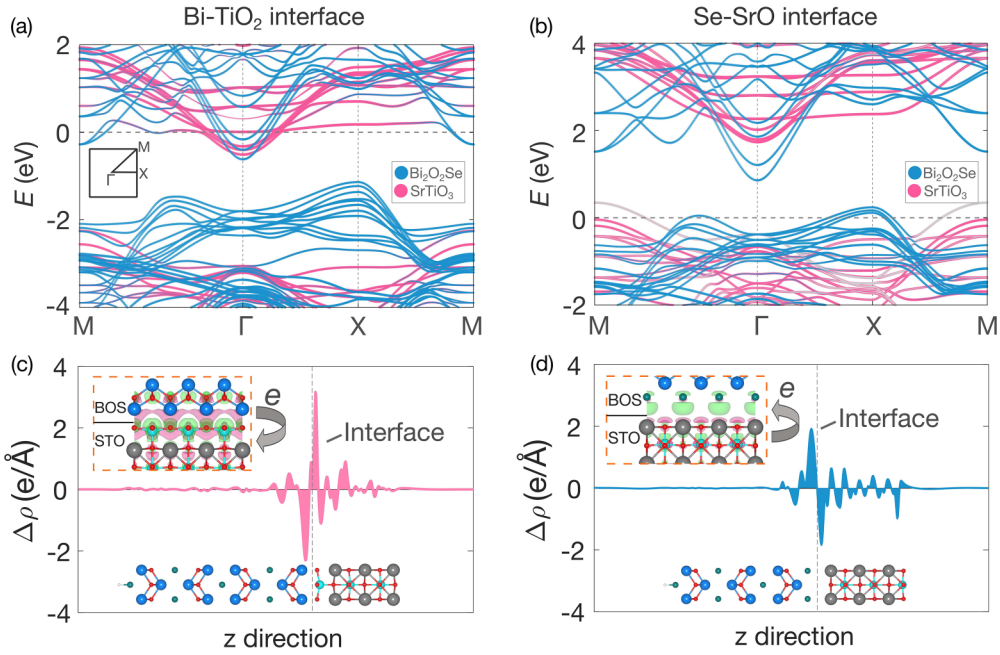

FIG. 2. (a), (b) Density functional theory (DFT) calculated electronic band structures of ideal BOS/STO interface with [Bi-TiO_2] and [Se-SrO] contact types. The inset in (a) is the corresponding reciprocal space path. The Fermi level is set to energy zero. The gray lines in (b) denote that the corresponding electronic states derive from the surface states of the STO slab on the opposite side of the interface. (c,d) Planar averaged electron density differences of the [Bi-TiO_2] (c) and [Se-SrO] (d) contact types with respect to isolated slabs, which are calculated as $\Delta\rho = \rho_{\mathrm{BOS/STO}} - \rho_{\mathrm{BOS}} - \rho_{\mathrm{STO}}$. For ease of visualization, the horizontal-axis values of the plots are indicated by the corresponding locations in the bottom inset slab structures along the z direction, that is, the direction perpendicular to the interface. The upper inset figures in dashed boxes are plots of charge density differences, drawn using the VESTA software [34]. The green (pink) color corresponds to charge accumulation (depletion) and the isosurfaces correspond to $\Delta\rho$ equal to 0.0015 $e/\text{Å}^3$.

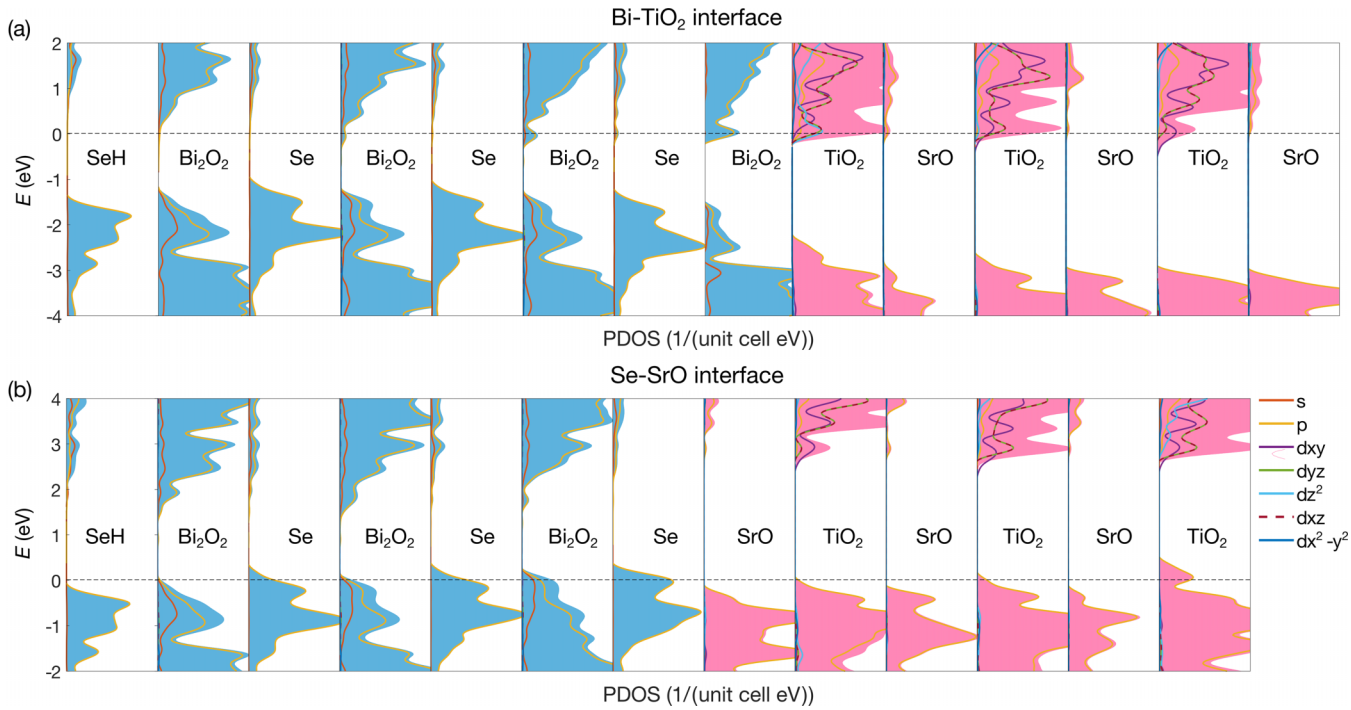

FIG. 3. Layer-by-layer projected density of states (PDOS) for the BOS/STO heterostructural models in Figs. 1(c) and 1(d). The top (a) and bottom (b) panels correspond to the [Bi-TiO_2] and [Se-SrO] contact types, respectively. The color lines indicate the contributions of different atomic orbitals (s, p, d_{xy}, d_{yz}, d_{z^2}, d_{xz}, and $d_{x^2-y^2}$) to the PDOS of each atomic layer.

the valence bands of both BOS and STO, indicating a reverse direction of charge transfer from STO to BOS.

The different charge transfer behavior is confirmed by explicitly computing the amount of interfacial charge transfer at the two types of BOS/STO interfaces. As shown in Figs. 2(c) and 2(d), charge accumulation and depletion on the side of STO are found in the [Bi-TiO_2] and [Se-SrO] contact types, respectively. In addition to the opposite charge transfer direction, the magnitude of charge transfer is significantly different between the two. Bader charge analysis [38] reveals that about 0.5 electron per 2D unit cell (*e*/u.c) is transferred from BOS to STO in the [Bi-TiO_2] contact type, whereas the corresponding number is 0.2 *e*/u.c from STO to BOS in the [Se-SrO] contact type. The stronger interfacial charge transfer and electronic hybridization observed at the [Bi-TiO_2] contact interface explain its higher interfacial binding energy than the [Se-SrO] contact type, as discussed in the previous section.

We have further studied the dependence of interfacial charge transfer on the the number of BOS layers in BOS/STO heterostructures. It is found that, even if the number of BOS layers is reduced one (monolayer), there is still interfacial charge transfer at the BOS/STO interface, and the amount of transferred charge does not change much, as shown in Supplemental Fig. S8. Thus, for BOS/STO heterostructures, there is no critical thickness of BOS layers for the appearance of interfacial charge transfer. As mentioned in the Methods section, in our BOS/STO heterostructural model, we use hydrogen passivation of a full Se surface layer [Figs. 1(c) and 1(d)] to simulate the experimentally observed BOS surface with 50% of Se coverage. The BOS slabs constructed in this way are already in metallic state before in contact with STO slabs [Supplemental Figs. S6(b,c)], and charge transfer between BOS and STO is expected to occur regardless of the BOS layer thickness.

Even if we adopt a BOS/STO heterostructural configuration with full surface Se coverage (no hydrogen passivation) for the [Bi-TiO_2] contact type, a model setup that is more similar to the *n*-type LAO/STO heterostructural model studied by Lee and Demkov [37], we find that there is still no critical BOS layer thickness of interfacial charge transfer. In their first-principles study, Lee and Demkov find that the critical thickness of LAO layers to introduce interfacial charge transfer at the *n*-type LAO/STO interface is ∼13 Å (three and a half unit cells). The charge transfer occurs when the internal electric field in the LAO layers raises the electrostatic potential energy to such a level that the VBM of the LAO layer near the vacuum surface becomes higher than the CBM of STO [37]. Thus, the critical thickness in the polarization doping model of Lee and Demkov depends crucially on the band alignment of the two materials at interface. Adopting symmetric $(BOS)_m/(STO)_n/(BOS)_m$ slab models (*m*, *n* representing the number of unit cells in each component) with full surface Se coverage and no surface hydrogen termination, as well as the GGA $+U$ method ($U = 4.36$ eV), our calculation results show that even with one BOS layer, charge transfer from BOS to STO already exists (Fig. S9 and Fig. S10), as the VBM of BOS in the heterostructure is already higher than the CBM of STO. This is because the VBM of both STO and LAO mainly derive from the oxygen $2p$ orbitals, whereas the VBM of BOS mainly derives from the $4p$ orbitals of Se [1,7]. The Se $4p$ orbital is higher in energy than the oxygen $2p$ orbital [39], and as a result the VBM of BOS is much closer to the CBM of STO than the VBM of LAO.

We note, however, that the first-principles band structures corresponding to full surface Se coverage is inconsistent with the experimentally measured electronic structure of bilayer BOS films grown on TiO_2-terminated STO substrates by molecular beam epitaxy, as measured by angle-resolved photoemission spectroscopy (ARPES) in Ref. [11]. The ARPES result indicates that the valence band of bilayer BOS grown on STO is fully occupied while the conduction band is partially occupied. In contrast, the first-principles DFT+U band structure of the BOS/STO heterostructural with full surface Se coverage [Fig. S9(d)] indicates that the Fermi level crosses the valence band of BOS. Supplemental Fig. S11 also shows that, in stoichiometric BOS slabs with full surface Se coverage on one side, dielectric breakdown (bandgap closing) already occurs in bilayer BOS, as a result of the internal electric field arising from the electric dipole of the slab, as well as the small bandgap of BOS (∼0.5 eV in DFT and ∼0.8 eV in experiment). Furthermore, Se vacancies in BOS are known to be electron donors and have low formation energies [40]. With non-full surface Se coverage on one side and Bi_2O_2 layer on the other, the bandgap of bilayer BOS will open up again (due to reduced internal electric field) and the Fermi level will move into the conduction band (due to the electron doping by Se vacancies), as shown by the first-principles band structures in Supplemental Fig. S12.

In addition, we have investigated the existence of an internal electric field inside the BOS slabs of the *n*-type BOS/STO heterostructures, which could originate from the symmetry breaking at the interface and the alternate postive and negative charged layers of Bi_2O_2 and Se in BOS. To this end, we employ symmetric $(BOS)_m/(STO)_n/(BOS)_m$ slab models with surface hydrogen passivation ($n = 6.5$, $m = 3$, 4, and 5). Following Refs. [18,37], the internal electric field was calculated by computing the average electrostatic potential energies across the whole simulation cells of $(BOS)_m/(STO)_n/(BOS)_m$ slabs. The results, shown in Fig. S13, indicates the existence of an internal electric field of ∼0.017 V/Å in the BOS slabs. This value is significantly smaller than the corresponding value inside the LAO layers of *n*-type LAO/STO heterostructures (0.24 V/Å, Ref. [37]). The much smaller internal electric field could originate from the fact that surface hydrogen passivation (half-full surface Se coverage) leads to smaller electric polarization in the BOS slabs. Moreover, the observation that metallic electron carriers in the BOS/STO heterostructures are not as strongly localized at the interface as in LAO/STO heterostructures, as indicated by the layer-by-layer PDOS in Fig. 3(a), could result in more effective screening of the internal electric field.

IV. DISCUSSIONS

The intriguing electronic properties of the BOS/STO interfaces originate from polar discontinuity at the contact interfaces. Unlike vdW layered materials such as MoS_2, BOS consists of alternate stacking of the charged $[Bi_2O_2]^{2+}$ and $[Se]^{2-}$ layers along the [001] direction. Each Bi_2O_2 layer donates two electrons per 2D unit cell to the neighboring Se

layers, resulting in interlayer electrostatic interaction between the $[Bi_2O_2]^{2+}$ and $[Se]^{2-}$ layers. Here, the nominal charge of Bi, O, and Se are 3+, 2−, and 2− in the simple ionic limit, respectively. In comparison, STO has alternate stacking of charge neutral TiO_2 and SrO layers along the [001] direction, with the nominal charges of Ti, Sr, O being 4+, 2+, and 2− in the simple ionic limit, respectively. Hence, along the [001] direction, BOS is polar while STO is not, and as a result, there is a polar discontinuity at the interface between BOS and STO, similar to that at the LAO/STO interface [5,12,41]. For the [Bi-TiO_2] contact type of the BOS/STO interface, the polar discontinuity can be denoted as $(Bi_2O_2)^{2+}/(TiO_2)^0$, while for the [Se-SrO] contact type, it can be denoted as $(Se)^{2-}/(SrO)^0$.

In the absence of interfacial electronic or atomic reconstruction, polar discontinuity at heterostructural interface can lead to "polar catastrophe", where the electrostatic potential generated by the charged layers grows quickly away from the interface and diverges in the bulk limit [41–43]. In heterostructures formed by growing a conventional polar semiconductor on a nonpolar semiconductor, such as GaAs on Si, such potential divergence is avoided via atomic reconstruction at the interface through atomic disordering or a change in stoichiometry [44–46]. However, in oxide heterostructures where certain ions can assume multiple valencies, such as Ti in STO, whose valence can change from Ti^{4+} to Ti^{3+}, polar catastrophe can be avoided via electronic reconstruction, specifically through interfacial charge transfer that leads to mixed valencies of certain ions [41–43]. Such interfacial electronic construction was considered to be responsible for the observation of 2D electron gas at the $(LaO)^+/(TiO_2)^0$ interface between LAO and STO [5].

The interfacial electronic properties of the BOS/STO interfaces share certain similarities with the LAO/STO interfaces. The polar discontinuity of the [Bi-TiO_2] contact interface, explicitly written as $(Bi_2O_2)^{2+}/(TiO_2)^0$, corresponds to that of the $(LaO)^+/(TiO_2)^0$ interface between LAO and STO. After electronic reconstruction in self-consistent DFT calculations, this interface type involves charge transfer from the Bi_2O_2 layer to the TiO_2 layer in the amount of ∼0.5 *e*/u.c., as illustrated in Fig. 4(a). Conceptually, one can also start from the atomic limit and then allow ionization of the elements. In bulk BOS, a Bi_2O_2 layer donates 2 *e*/u.c. of electrons to its two neighboring Se layers. However, for the Bi_2O_2 layer at the Bi_2O_2/TiO_2 interface, only one Se layer on one side of the interface is available to accept electrons. Hence, the Bi_2O_2 layer at the interface have excess electrons on the order of 1 *e*/u.c, which leads to an *n*-type interface. These excess electrons can be partially transferred to the TiO_2 layer on the other side of the interface, in the process partially changing the Ti valency from Ti^{4+} to Ti^{3+}.

On the other hand, the polar discontinuity at the [Se-SrO] contact interface, written as $(Se)^{2-}/(SrO)^0$, is akin to the $(AlO_2)^-/(SrO)^0$ interface between LAO and STO. In this case, the Se layer at the interface only has one neighboring Bi_2O_2 layer from which it can receive electrons, leading to a *p*-type electronic state. This electron deficiency could be mitigated by charge transfer from the SrO layer on the STO side of the interface. However, since it is energetically costly to induce mixed valency for either Sr or O, the amount of charge transfer from the SrO layer is rather limited. In our

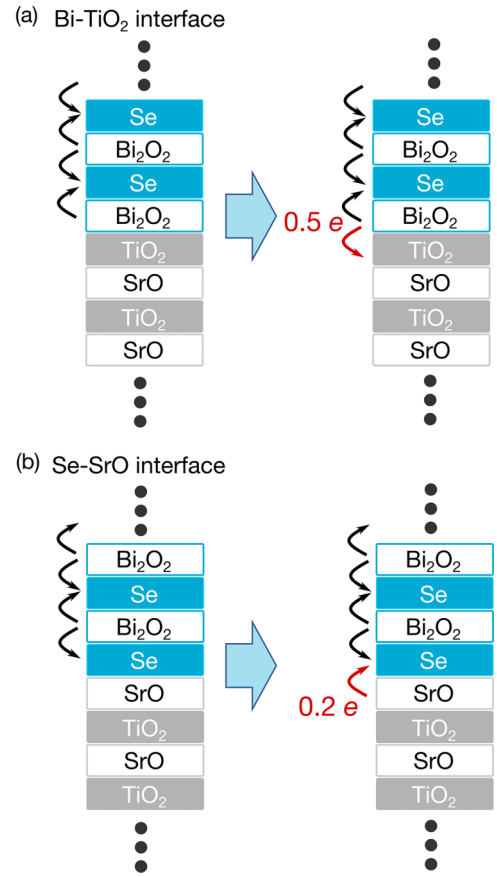

FIG. 4. Schematic diagrams of polar discontinuities and charge transfer at the interfaces between BOS and STO. (a) The [Bi-TiO_2] contact interface. (b) The [Se-SrO] contact interface.

DFT calculation of the ideal [Se-SrO] interface, the amount of charge transfer is calculated to be ∼0.2 *e*/u.c., as illustrated in Fig. 4(b). In fact, we find that the transferred charge in our DFT calculation mainly originates from the surface state of the STO slab on the opposite side of the contact interface, as can be seen from the layer-by-layer PDOS in Fig. 3(b). Given that in real experiments, the SrO-terminated substrate is rather thick, charge transfer from the STO side to the BOS side would be further hampered. Since electronic reconstruction at the [Se-SrO] contact interface is energetically unfavorable, atomic reconstruction is expected to occur in this contact type in real systems, where the generation of Se vacancies or O vacancies near the interface could provide the extra electrons that compensate the *p*-type carriers. Indeed, in the *p*-type $(AlO_2)^-/(SrO)^0$ interface between LAO and STO, oxygen vacancies play a central role in avoiding polar catastrophe and lead to an insulating interface instead of *p*-type hole transport [5,42]. Similar phenomena could happen at the [Se-SrO] contact type of the BOS/STO interface.

While there is similarity between the BOS/STO and LAO/STO interfaces in terms of polar discontinuity, there are also important differences between the two systems. As mentioned earlier, the VBM of BOS primarily derives from the 4*p* orbitals of the Se atoms, whereas the VBM of both STO and LAO mainly derive from the 2*p* orbitals of oxygen atoms.

The latter leads to a small valence band offset of ∼0.2 eV between STO and LAO [47]. Due to the higher orbital energy of the Se $4p$ orbital than the oxygen $2p$ orbital, in n-type BOS/STO interface, the VBM of BOS is estimated to be at least 1 eV higher than that of STO, which leads to a much smaller offset between the VBM of BOS and CBM of STO. As a result, the polarization field in a BOS slab can easily elevate the VBM of BOS above the CBM of STO, leading to the absence of a critical thickness in interfacial charge transfer in BOS/STO heterostructural models with full surface Se coverage, as observed in our simulation. In addition, the bandgap of BOS is much smaller than that of LAO. The experimental bandgap of BOS is ∼0.8 eV [2], while that of LAO is 5.6 eV [37]. Therefore, the internal electric field in a nonsymmetric BOS slab can more easily lead to its dielectric breakdown, indicating that the thick, nonsymmetric BOS slab with a Bi_2O_2 layer on one side and full Se layer on the other side is energetically unfavorable, which is consistent with the experimental observation that cleaved BOS sample surfaces have ∼50% of Se vacancies [2]. These Se vacancies are electron donors that spontaneously ionize and do not introduce in-gap states [2,40], and their presence plays a key role in the consideration of interfacial charge transfer in BOS/STO heterostructures, as we show in our work. We expect that these features are generalizable to the interface between BOS and other perovskite oxides.

It is worth emphasizing that the polar discontinuities of the BOS/STO interfaces arise from the charged layered structure of BOS with interlayer electrostatic interaction, which is absent in heterostructures of typical vdW layered materials such as MoS_2 grown on STO. Consequently, the substrate used for growing BOS thin films could have a significant influence on their experimentally measured electronic properties. When mica substrates are used for the CVD growth of BOS [1], the interfacial structure involves the surface K^+ layer of mica in contact with the Se layer of BOS, as illustrated in Fig. 5(a), which has been experimentally observed using atomic-scale scanning transmission electron microscopy [48]. Since the K^+ layer of mica is electronically inert, charge transfer between BOS and mica shall be minimal. By contrast, for BOS thin films grown on TiO_2-terminated STO substrates, the interface belongs to the [Bi-TiO_2] contact type [10,11], as schematically depicted in Fig. 5(b). As we have discussed above, due to polar discontinuity and the ability of Ti^{4+} to undergo valence change, significant interfacial charge transfer from BOS to STO is expected to occur. Consequently, the electronic states responsible for the n-type electron transport have contributions from both BOS and STO. As the electron effective mass of STO is larger than that of BOS [see also Fig. 2(a)], the resulting measured room-temperature electron mobility of BOS grown on TiO_2-terminated STO substrates shall be smaller than those measured from BOS samples grown on mica substrates, which was indeed found in experiments [10]. Nonetheless, the strong interfacial interaction means that novel electronic or magnetic properties could emerge from the [Bi-TiO_2] contact type of the BOS/STO interface, as in the case of LAO grown on TiO_2-terminated STO substrates [12].

For the [Se-SrO] contact configuration, the interfacial charge transfer is much weaker, resulting in a weakly p-type electronic structure and energetically well-separated

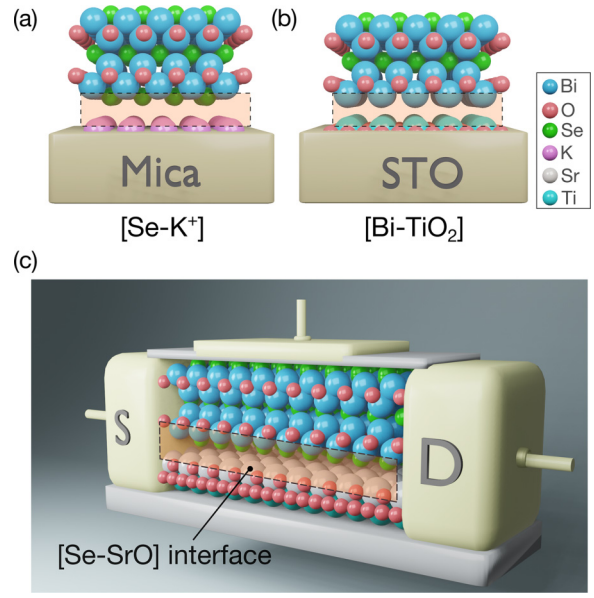

FIG. 5. (a), (b) Illustration of the contact interface of BOS thin films grown on a mica and TiO_2-terminated STO substrates. (c) Schematic illustration of a field-effect transistor device directly fabricated on a BOS layer grown on a SrO-terminated STO substrate, with the [Se-SrO] contact interface indicated by orange shade.

conduction bands of BOS and STO [Fig. 2(b)]. Although the formation of Se vacancies and possibly oxygen vacancies, promoted by the polar discontinuity at the interface, are likely to compensate the hole carriers, the p-type behavior before reconstruction suggests that field-effect transistors fabricated from BOS layers grown on SrO-terminated STO substrate, as illustrated in Fig. 5(c), may circumvent the problem of high residual electron carrier concentrations that has plagued BOS-based transistor devices [49], and may even pave the way for realizing p-type transistors based on BOS.

V. CONCLUSIONS

In conclusion, we have performed systematic first-principles investigations of the energetic and electronic properties of ideal BOS/STO interfaces, revealing the crucial effect of interfacial contact type and polar discontinuity on the interfacial properties. For BOS grown on TiO_2-terminated STO, a Bi_2O_2 layer in contact with a surface TiO_2 layer of STO, denoted by [Bi-TiO_2], is found to be the lowest-energy interface configuration, in consistent with experimental observations. Due to the polar discontinuity between BOS and STO and the ability of titanium ions to exist in mixed valencies, a significant charge transfer from BOS to STO occurs in the [Bi-TiO_2] contact type. This leads to an n-type interface with a mixed metallic state of BOS and STO, which is likely responsible for the lower electron mobility observed in BOS grown on TiO_2-terminated STO substrates as compared to BOS grown on electronically more inert substrates such as mica. For SrO-terminated STO substrates, we find that the lowest-energy contact configuration between BOS and STO is a Se layer on a SrO layer, denoted by [Se-SrO]. This contact configuration has a much weaker interfacial charge transfer,

resulting in a *p*-type electronic structure. The asymmetry in interfacial charge transfer properties between [Bi-TiO_2] and [Se-SrO] interfaces can be explained in terms of the ability of Ti^{4+} to undergo a change in valence to Ti^{3+} in a TiO_2 layer, whereas such a change in valence is energetically costly for Sr^{2+} or O^{2-} in a SrO layer. In real experiments, the hole carriers at the [Se-SrO] interface may be compensated by ionized Se or oxygen vacancies. However, the energetically well-separated conduction bands of BOS and STO in this contact type suggests that the excellent electron transport properties of BOS may be better preserved in this contact type. These results indicate that BOS grown on TiO_2-terminated STO substrates could be a fruitful system for exploring emergent interface phenomena between an oxychalcogenide and an oxide, whereas SrO-terminated STO substrates may be desirable for wafer-scale growth of BOS films with excellent carrier transport properties.

ACKNOWLEDGMENTS

This work is supported by the National Natural Science Foundation of China (NSFC) under Projects No. 62004172 and No. 62374136. W.L. also acknowledges the support by Research Center for Industries of the Future (RCIF) at Westlake University under Award No. WU2022C041. X.L. and X.Z. thank the Westlake Multidisciplinary Research Initiative Center (MRIC) under Grant No. MRIC20200402. The authors thank S. Zhao and X. Yao for helpful discussions, as well as the High-Performance Computing Center of Westlake University for technical assistance.

[1] J. Wu, H. Yuan, M. Meng, C. Chen, Y. Sun, Z. Chen, W. Dang, C. Tan, Y. Liu, J. Yin, Y. Zhou, S. Huang, H. Q. Xu, Y. Cui, H. Y. Hwang, Z. Liu, Y. Chen, B. Yan, and H. Peng, High electron mobility and quantum oscillations in non-encapsulated ultrathin semiconducting Bi_2O_2Se, Nat. Nanotechnol. **12**, 530 (2017).

[2] C. Chen, M. Wang, J. Wu, H. Fu, H. Yang, Z. Tian, T. Tu, H. Peng, Y. Sun, X. Xu, J. Jiang, N. B. M. Schröter, Y. Li, D. Pei, S. Liu, S. A. Ekahana, H. Yuan, J. Xue, G. Li, J. Jia *et al.*, Electronic structures and unusually robust bandgap in an ultrahigh-mobility layered oxide semiconductor, Bi_2O_2Se, Sci. Adv. **4**, eaat8355 (2018).

[3] J. Yin, Z. Tan, H. Hong, J. Wu, H. Yuan, Y. Liu, C. Chen, C. Tan, F. Yao, T. Li, Y. Chen, Z. Liu, K. Liu, and H. Peng, Ultrafast and highly sensitive infrared photodetectors based on two-dimensional oxyselenide crystals, Nat. Commun. **9**, 3311 (2018).

[4] T. Li and H. Peng, 2D Bi_2O_2Se: An emerging material platform for the next-generation electronic industry, Acc. Mater. Res. **2**, 842 (2021).

[5] A. Ohtomo and H. Y. Hwang, A high-mobility electron gas at the $LaAlO_3/SrTiO_3$ heterointerface, Nature (London) **427**, 423 (2004).

[6] N. Petrone, C. R. Dean, I. Meric, A. M. van der Zande, P. Y. Huang, L. Wang, D. Muller, K. L. Shepard, and J. Hone, Chemical vapor deposition-derived graphene with electrical performance of exfoliated graphene, Nano Lett. **12**, 2751 (2012).

[7] Z. Zhu, X. Yao, S. Zhao, X. Lin, and W. Li, Giant modulation of the electron mobility in semiconductor Bi_2O_2Se via incipient ferroelectric phase transition, J. Am. Chem. Soc. **144**, 4541 (2022).

[8] Z. Xu, J. Wang, T. Wang, W. Hu, X. Yang, and X. Lin, Huge permittivity and premature metallicity in Bi_2O_2Se single crystals, Sci. China Phys. Mech. **64**, 267312 (2021).

[9] T. Li, T. Tu, Y. Sun, H. Fu, J. Yu, L. Xing, Z. Wang, H. Wang, R. Jia, J. Wu, C. Tan, Y. Liang, Y. Zhang, C. Zhang, Y. Dai, C. Qiu, M. Li, R. Huang, L. Jiao, K. Lai *et al.*, A native oxide high-κ gate dielectric for two-dimensional electronics, Nat. Electron. **3**, 473 (2020).

[10] C. Tan, M. Tang, J. Wu, Y. Liu, T. Li, Y. Liang, B. Deng, Z. Tan, T. Tu, Y. Zhang, C. Liu, J.-H. Chen, Y. Wang, and H. Peng, Wafer-scale growth of single-crystal 2D semiconductor on perovskite oxides for high-performance transistors, Nano Lett. **19**, 2148 (2019).

[11] Y. Liang, Y. Chen, Y. Sun, S. Xu, J. Wu, C. Tan, X. Xu, H. Yuan, L. Yang, Y. Chen, P. Gao, J. Guo, and H. Peng, Molecular beam epitaxy and electronic structure of atomically thin oxyselenide films, Adv. Mater. **31**, 1901964 (2019).

[12] H. Y. Hwang, Y. Iwasa, M. Kawasaki, B. Keimer, N. Nagaosa, and Y. Tokura, Emergent phenomena at oxide interfaces, Nat. Mater. **11**, 103 (2012).

[13] P. E. Blöchl, Projector augmented-wave method, Phys. Rev. B **50**, 17953 (1994).

[14] G. Kresse and J. Furthmüller, Efficient iterative schemes for *ab initio* total-energy calculations using a plane-wave basis set, Phys. Rev. B **54**, 11169 (1996).

[15] J. P. Perdew, K. Burke, and M. Ernzerhof, Generalized gradient approximation made simple, Phys. Rev. Lett. **77**, 3865 (1996).

[16] V. I. Anisimov, J. Zaanen, and O. K. Andersen, Band theory and Mott insulators: Hubbard U instead of Stoner I, Phys. Rev. B **44**, 943 (1991).

[17] S. L. Dudarev, G. A. Botton, S. Y. Savrasov, C. J. Humphreys, and A. P. Sutton, Electron-energy-loss spectra and the structural stability of nickel oxide: An LSDA+U study, Phys. Rev. B **57**, 1505 (1998).

[18] W. Li, L. Gao, and A. A. Demkov, Controlling spin-polarized carriers at the $SrTiO_3$/EuO interface via the ferroelectric field effect, Phys. Rev. B **102**, 035308 (2020).

[19] Y. A. Abramov, V. G. Tsirelson, V. E. Zavodnik, S. A. Ivanov, and I. D. Brown, The chemical bond and atomic displacements in $SrTiO_3$ from x-ray diffraction analysis, Acta. Crystallogr. B **51**, 942 (1995).

[20] See Supplemental Material at http://link.aps.org/supplemental/10.1103/PhysRevB.108.245304 for Supplemental Figs. S1 to S13.

[21] L. Bengtsson, Dipole correction for surface supercell calculations, Phys. Rev. B **59**, 12301 (1999).

[22] H. J. Monkhorst and J. D. Pack, Special points for Brillouin-zone integrations, Phys. Rev. B **13**, 5188 (1976).

[23] H. Boller, Die kristallstruktur von Bi_2O_2Se, Monats. Chem. **104**, 916 (1973).

[24] R. Hoffmann and C. Zheng, Making and breaking bonds in the solid state: The $ThCr_2$ Si_2 structure, J. Phys. Chem. **89**, 4175 (1985).

[25] A. L. J. Pereira, D. Santamaría-Pérez, J. Ruiz-Fuertes, F. J. Manjón, V. P. Cuenca-Gotor, R. Vilaplana, O. Gomis, C. Popescu, A. Muñoz, P. Rodríguez-Hernández, A. Segura, L. Gracia, A. Beltrán, P. Ruleova, C. Drasar, and J. A. Sans, Experimental and theoretical study of Bi_2O_2Se under compression, J. Phys. Chem. C **122**, 8853 (2018).

[26] Q. Wei, R. Li, C. Lin, A. Han, A. Nie, Y. Li, L.-J. Li, Y. Cheng, and W. Huang, Quasi-two-dimensional Se-terminated bismuth oxychalcogenide (Bi_2O_2Se), ACS Nano **13**, 13439 (2019).

[27] T. Björkman, A. Gulans, A. V. Krasheninnikov, and R. M. Nieminen, Are we van der Waals ready? J. Phys.: Condens. Matter **24**, 424218 (2012).

[28] M. Huijben, A. Brinkman, G. Koster, G. Rijnders, H. Hilgenkamp, and D. H. A. Blank, Structure-property relation of $SrTiO_3/LaAlO_3$ interfaces, Adv. Mater. **21**, 1665 (2009).

[29] M. Kawasaki, K. Takahashi, T. Maeda, R. Tsuchiya, M. Shinohara, O. Ishiyama, T. Yonezawa, M. Yoshimoto, and H. Koinuma, Atomic control of the $SrTiO_3$ crystal surface, Science **266**, 1540 (1994).

[30] G. Koster, B. L. Kropman, G. J. H. M. Rijnders, D. H. A. Blank, and H. Rogalla, Quasi-ideal strontium titanate crystal surfaces through formation of strontium hydroxide, Appl. Phys. Lett. **73**, 2920 (1998).

[31] T. Ohnishi, K. Shibuya, M. Lippmaa, D. Kobayashi, H. Kumigashira, M. Oshima, and H. Koinuma, Preparation of thermally stable TiO_2-terminated $SrTiO_3$ (100) substrate surfaces, Appl. Phys. Lett. **85**, 272 (2004).

[32] R. Bachelet, F. Sánchez, F. J. Palomares, C. Ocal, and J. Fontcuberta, Atomically flat SrO-terminated $SrTiO_3$ (001) substrate, Appl. Phys. Lett. **95**, 141915 (2009).

[33] M. Radovic, N. Lampis, F. M. Granozio, P. Perna, Z. Ristic, M. Salluzzo, C. M. Schlepütz, and U. S. di Uccio, Growth and characterization of stable SrO-terminated $SrTiO_3$ surfaces, Appl. Phys. Lett. **94**, 022901 (2009).

[34] K. Momma and F. Izumi, Vesta 3 for three-dimensional visualization of crystal, volumetric and morphology data, J. Appl. Cryst. **44**, 1272 (2011).

[35] K. van Benthem, C. Elsässer, and R. H. French, Bulk electronic structure of $SrTiO_3$: Experiment and theory, J. Appl. Phys. **90**, 6156 (2001).

[36] Y.-Y. Pai, A. Tylan-Tyler, P. Irvin, and J. Levy, Physics of $SrTiO_3$-based heterostructures and nanostructures: A review, Rep. Prog. Phys. **81**, 036503 (2018).

[37] J. Lee and A. A. Demkov, Charge origin and localization at the *n*-type $SrTiO_3/LaAlO_3$ interface, Phys. Rev. B **78**, 193104 (2008).

[38] G. Henkelman, A. Arnaldsson, and H. Jónsson, A fast and robust algorithm for Bader decomposition of charge density, Comput. Mater. Sci. **36**, 354 (2006).

[39] H. B. Gray, *Electrons and Chemical Bonding* (W. A. Benjamin, Reading, MA, 1965).

[40] H. Fu, J. Wu, H. Peng, and B. Yan, Self-modulation doping effect in the high-mobility layered semiconductor Bi_2O_2Se, Phys. Rev. B **97**, 241203(R) (2018).

[41] J. Mannhart, D. Blank, H. Hwang, A. Millis, and J.-M. Triscone, Two-dimensional electron gases at oxide interfaces, MRS Bull. **33**, 1027 (2008).

[42] N. Nakagawa, H. Y. Hwang, and D. A. Muller, Why some interfaces cannot be sharp, Nat. Mater. **5**, 204 (2006).

[43] H. Y. Hwang, Tuning interface states, Science **313**, 1895 (2006).

[44] G. A. Baraff, J. A. Appelbaum, and D. R. Hamann, Self-consistent calculation of the electronic structure at an abrupt GaAs-Ge interface, Phys. Rev. Lett. **38**, 237 (1977).

[45] W. A. Harrison, E. A. Kraut, J. R. Waldrop, and R. W. Grant, Polar heterojunction interfaces, Phys. Rev. B **18**, 4402 (1978).

[46] H. Kroemer, Polar-on-nonpolar epitaxy, J. Cryst. Growth **81**, 193 (1987).

[47] M. Choi, C. Lin, M. Butcher, C. Rodriguez, Q. He, A. B. Posadas, A. Y. Borisevich, S. Zollner, and A. A. Demkov, Quantum confinement in transition metal oxide quantum wells, Appl. Phys. Lett. **106**, 192902 (2015).

[48] C. Hong, Y. Tao, A. Nie, M. Zhang, N. Wang, R. Li, J. Huang, Y. Huang, X. Ren, Y. Cheng, and X. Liu, Inclined ultrathin Bi_2O_2Se films: A building block for functional van der Waals heterostructures, ACS Nano **14**, 16803 (2020).

[49] T. Wang, Z. Xu, Z. Zhu, M. Wu, Z. Lou, J. Wang, W. Hu, X. Yang, T. Sun, X. Zheng, W. Li, and X. Lin, Highly insulating phase of Bi_2O_2Se thin films with high electronic performance, Nano Res. **16**, 3224 (2023).